Inverse Modeling of Nitrogen Oxides Emissions from the 2010 Russian Wildfires by Using Satellite Measurements of Nitrogen Dioxide

Evgeny V. Berezin [1], Igor B. Konovalov [1],* and Yulia Y. Romanova [2]

Published: 15 July 2016

[1] Institute of Applied Physics, Russian Academy of Sciences, 46 Ulyanov Str., Nizhniy Novgorod, 603950, Russia; e.berezin@appl.sci-nnov.ru, konov@appl.sci-nnov.ru
[2] Institute for Physics of Microstructures, Russian Academy of Sciences, Afonino, 7 Academicheskaya Str., Nizhniy Novgorod, 603087, Russia; jul@ipm.sci-nnov.ru
* Correspondence: konov@appl.sci-nnov.ru; Tel.: +7-905-192-6335

Abstract: Nitrogen oxides (NO_x) play a major role in the atmospheric oxidation processes leading to ozone and secondary organic aerosol formation in the lower atmosphere. Wildfires are one of the important sources of NO_x emissions; however, knowledge of NO_x emissions from fires is currently insufficient and available estimates provided by emission inventories have mostly not been validated against atmospheric measurements. Recent studies indicated that useful observational constraints to biomass burning (BB) NO_x emissions are provided by satellites measurements of nitrogen dioxide (NO_2), but available BB NO_x emission estimates inferred from such measurements involve quantitative assumptions regarding the atmospheric NO_x lifetime. In this study, we investigated NO_x emissions from the extreme wildfires that occurred in the European part of Russia in summer 2010. To this end, we analyzed tropospheric NO_2 retrievals from measurements performed by the OMI satellite instrument in the framework of an original inverse modeling method. A quantitative relationship between BB NO_x emissions and tropospheric NO_2 columns was simulated using the mesoscale CHIMERE chemistry transport model. Our analysis indicated that such a relationship depends strongly on BB emissions of volatile organic compounds and that a dependence of the effective NO_x lifetime on the NO_x fluxes can be essentially nonlinear. Our estimates of the total NO_x emissions in the study region are found to be at least 40% larger compared to the respective data from the GFASv1.0 and GFED4.1s global fire emission inventories.

Keywords: nitrogen oxides; wildfires; satellite measurements; chemistry transport model; inverse modeling; biomass burning emissions

1. Introduction

Nitrogen oxides ($NO_x=NO+NO_2$) are important atmospheric constituents affecting climate processes and air quality specifically by serving as precursors of tropospheric ozone [1,2] and influencing secondary aerosol formation [3,4]. One of the significant sources of NO_x on a global scale is associated with biomass burning (BB), including wildfires: it is estimated that biomass and biofuel burning provide around 15 % of NO_x emissions globally [5]. On a regional scale, BB NO_x emissions can dominate in oxidation processes leading to ozone formation inside smoke plumes from by wildfires [6] over other NO_x sources and provide a major contribution to NO_2 column amounts over fire spots [7].

Despite the important role played by BB NO_x emissions in atmospheric processes, current knowledge regarding the amounts of NO_x emitted into the atmosphere from wildfires is insufficient. Available BB NO_x emission estimates provided by "bottom-up" fire emission inventories [e.g., 8, 9] based on indirect measurements of the amounts of biomass burned have mostly not been validated against atmospheric measurements and are likely to be rather uncertain as indicated by a diversity of NO_x emission factors involved in such inventories and reported in literature for similar types of vegetation cover [10]. Validation of BB NO_x emission estimates is more difficult compared to validation of BB emissions of some other species (such as, e.g. CO) particularly due to high reactivity and a relatively short atmospheric lifetime of NO_x, leading to a strong variability of NO_x concentration in space and time.

Nonetheless, several studies [7,11-14] have recently examined the relationship between satellite-retrieved fire radiative power (FRP) and tropospheric NO_2 columns over fire spots and reported reasonable estimates of fire emission rates (FER) [7,11] or emission coefficients (EC) [12-14], both of which allow one to calculate NO_x emissions, given the observed values of FRP. The measurement-based estimates of FER or EC for different regions and different types of bioma are useful, as they provide an insight into the capability of available parameterizations to capture spatial and temporal variability of NO_x emissions. However, such estimates are presently rather uncertain, particularly because they involve explicit quantitative assumptions regarding the NO_x lifetime and a NO_2/NO ratio. For example, it has been argued [13] that as the NO_x lifetime is likely to vary across individual fire plumes between 2 and 6 h, the estimates of EC can be uncertain at least by a factor of 3.

In this study, we also use FRP and NO_2 columns derived from satellite measurements, but unlike the previous studies, we do not make any explicit assumptions on the NO_x lifetime and a NO_2/NO ratio. Instead, we follow the inverse modeling approach that has earlier been successfully used [e.g., 15-18] to estimate anthropogenic NO_x emissions. Within this approach, the relationship between NO_2 columns and NO_x emissions can be simulated by a chemistry transport model, and the NO_x emissions (or related emission parameters) as well as the NO_x lifetime can be estimated by fitting simulated NO_2 columns to satellite data. The goals of our study were (1) to examine feasibility of using an inverse modeling method to estimate BB NO_x emissions in a region affected by numerous and intense wildfires, and (2) to assess an impact of chemical nonlinearities on the relationship between NO_2 columns over such a region and NO_x emissions from fires. We focused on the disastrous mega-fire event that took place in the European part of Russia in 2010. Emissions of some pollutants (such as CO and aerosol) from the Russian 2010 fires were already investigated using inverse methods (e.g. [19-21]), but, to the best of our knowledge, there have yet been no similar studies focusing on NO_x emissions from those fires.

2. Data and method

2.1. Input data

2.1.1. Satellite data

We used tropospheric NO_2 column amounts retrieved from measurements of visible and ultraviolet back scattered radiation by the OMI instrument [22] onboard the NASA EOS Aura satellite and provided by KNMI as the DOMINO version 2 data product [23,24]. OMI provides global coverage daily at the 13×24 km^2 nominal spatial resolution; the measurements are taken in the early afternoon, as the Aura satellite operates in a sun-synchronous polar orbit with an equator crossing at 13:45. The DOMINO version 2 data product was evaluated against ground-based (MAX-DOAS) measurements [25], and only a minor negative bias (~10 %) was found in the satellite data. Note that NO_2 data retrieved from OMI measurements (although with slightly different algorithms) were found to be useful in earlier studies of BB NO_x emissions [7,11,12,14].

Following recommendations of the data providers, potentially biased data retrieved for the scenes with the cloud fraction and surface albedo exceeding 30 % and 0.3, respectively, were disregarded. The details of the retrieval algorithm can be found elsewhere [23]. Note that the tropospheric NO_2 column retrieval procedure does not explicitly accounts for optical effects of BB aerosol. However, such effects were taken into account and corrected for in the same way as similar effects associated with clouds. Scenes strongly contaminated by cloud or aerosol were discarded, and so the bias is likely to remain limited (<20 %) [26]. The orbital NO_2 data available for the study period (that spans from 15 July to 16 August 2010) were projected onto a 0.5 by 0.5 degree rectangular grid covering the study region (48°–66° N; 20°–56° E). Any data falling to the same grid on the same day were averaged.

As a primary source of information on NO_x emissions from fires, we used the Fire Radiative Power (FRP) data [27,28] retrieved from satellite measurements of infrared radiation with the MODIS instruments operating onboard the Aqua and Terra satellites. Both the Aqua and Terra satellites are in a sun-synchronous polar orbits with corresponding equator overpass times of 13:30 and 10:30 LST (at daytime) and 01:30 and 22:30 LST (at nighttime). We used the standard MODIS Level 2 "thermal anomalies & fire" (MOD14 and MYD14, Collection 5) data product available free from the NASA Land Processes Distributed Active Archive Center [29]. The data were provided for each satellite overpass at the nominal 1×1 km^2 resolution. The same data have been widely used (e.g., [7, 9, 21]) to study fire emissions, and details about the retrieval algorithm and potential uncertainties can be found elsewhere [27].

Finally, our analysis involved satellite retrievals [30] of aerosol optical depth (AOD) at 550 nm wavelength. The measurements were also performed by the MODIS instruments onboard Aqua and Terra satellites. We used the Level 3 MYD08_D3/MOD08_D3 data product obtained from the NASA Giovanni-Interactive Visualization and Analysis system [30] in the framework of an earlier study [21]. The data had the spatial resolution of 1 by 1 degree and the temporal resolution of one day.

2.1.2 Simulation data

Along with NO_2 data derived from satellite measurements, we used NO_2 columns simulated with the CHIMERE chemistry transport model (CTM) [32]. The CHIMERE CTM is a typical Eulerian three-dimensional model enabling simulations of air pollution on various scales, from urban to continental ones. It takes into account major physical and chemical processes (including over 300 chemical and photochemical reactions) affecting the evolution of ~80 gaseous species in the lower atmosphere. It also enables simulations of aerosol species but simulated aerosol concentrations were not used in this study. In-detail description of the model structure and of parameterizations of physical and chemical processes is available elsewhere [32]. The model documentation and the source code can be downloaded from the CHIMERE website [33]. CHIMERE was successfully used in a number of studies, including those dedicated to investigations of atmospheric effects of wildfires (e.g., [19,21,34,35]).

The CHIMERE configuration was the same as in a previous study [21] of atmospheric impacts of the 2010 Russian wildfires that was focused on simulation of BB aerosol. Specifically, the simulations were performed with a horizontal resolution of 0.5°× 0.5° with the model grid covering most of European Russia and a portion of Eastern Europe (48°–66° N; 20°–56° E). In vertical, the model grid had 12 levels, with the top of the upper level fixed at 200 hPa.

Fire emissions were calculated using the emission model that had been successfully used and described in detail earlier [19,21,36]. Briefly, it assumes that BB emission rates, E, of any species in a given grid cell are proportional to the daily mean FRP values, Φ_d, that were inferred from daily maximum FRP values derived from the MODIS measurements (see Sect. 2.1.1) for a given grid cell:

$$E \sim \alpha\Phi_d \, , \qquad\qquad (1)$$

where α is a conversion factor from FRP to dry BB rate which is referred to below also as the FRP-to-BBR conversion factor and for which a "reference" value, α_r, of 0.368 kg s^{-1} MW^{-1} is adopted, taking into account the experimental data [37]. The relationship illustrated by Eq. (1) involves, in

particular, the emission factors for a given species region (see [21] and Table 1 therein), as well as the emission diurnal cycle that was derived for the study region (see [21] and Figure 1 therein) from the FRP measurements using a method developed earlier [35]. Details on the emission factor values and the emission diurnal cycle used in this study can be found elsewhere (see [21], Table 2 and Figure 1 therein).

A noteworthy feature of our simulations is that hourly values of the photolysis rates were calculated "offline" for each grid cell using the TUV model [38] and the satellite AOD data described in Sect. 2.1.1 (see also [19] for details of our calculations). CHIMERE runs were driven with meteorological data obtained from the WRF-ARW (v.3.6) model [39]. Further details on meteorological data, anthropogenic and biogenic emission data, and boundary conditions used in the CHIMERE runs performed in this study can be found elsewhere [21].

The model was run for the period from 12 July to 16 August 2010 both with and without fire emissions. Only the difference of nitrogen oxides concentrations from the two runs was considered in this study in order to minimize an impact of probable biases in biogenic and anthropogenic emissions on our estimates: such a difference was considered as a contribution of BB emissions to the nitrogen oxides concentrations. The first three days of the model runs were withheld from the analysis for model's spin-up.

The hourly BB NO_2 concentration data obtained from the CHIMERE runs were matched in time and space to the satellite NO_2 data and integrated vertically by applying the averaging kernels [40]. The averaging kernels provide information on contribution of different atmospheric layers to the tropospheric NO_2 column amounts retrieved from the OMI measurements and were available as a part of the DOMINO data product. The hourly BB NO_2 concentrations available for the same day and grid cell were averaged.

2.2. Method

Estimation of NO_x emissions was based on a general approach established in previous studies [19,21,36]. The idea is to optimize one or more parameters of the fire emission model by fitting modeled concentrations of a species considered to respective observations. Following one of the previous studies [21], we optimize the FRP- to-BBR conversion factor (α) by assuming that the same value of that factor is applicable to any types of vegetation land cover. Although, in reality, it is not necessarily true, large uncertainties in measurement and simulation data prevent us from obtaining estimates of α separately for individual biome types. Variability of the true values of α is expected to be taken into account in confidence intervals for our estimates.

In this study, the optimal value of α, α_{opt}, was inferred by fitting the NO_2 columns simulated with the CHIMERE model to those derived from the OMI observations:

$$\alpha_{opt} = \arg\min \sum_{i=1}^{Nd} \left(C_o^i - C_b^i - C_{mf}^i \right)^2, \qquad (2)$$

where C_o are the observed tropospheric NO_2 columns, C_b are the background parts of the tropospheric NO_2 columns (that is, the tropospheric NO_2 column amounts which would be present in the atmosphere if there were no fires and which are estimated as explained below), C_{mf} are the simulated tropospheric column amounts of NO_2 originating from fires and i is the index of a day. The NO_2 column amounts (C_o, C_b, C_{mf}) involved in Eq. (2) were obtained by averaging the corresponding spatially-distributed data for a given day over the study region.

To estimate the background NO_2 columns in a given grid cell (i) and in a given day (d), we considered the tropospheric NO_2 columns derived from the OMI measurements for the same grid cell but for another day chosen from the period from 15 July to 19 July 2010, when, according to our simulations, a contribution of fires to the mean NO_2 columns over the study region was negligible. If such "background" data were available for more than one day, a nearest, to d, day was selected. On the other hand, if there were no observational data for any of the days in the indicated period, then the given grid cell i was excluded from further analysis.

Eq. (2) was resolved iteratively. In each iteration, C_{mf}, was assumed to depend on BB NO_x emissions (and, thus, on α) linearly, that is:

$$\boldsymbol{C}_{mf}\left|\alpha = \alpha^{(n)}\right\rangle \cong \frac{\alpha^{(n)}}{\alpha^{(n-1)}}\boldsymbol{C}_{mf}\left|\alpha^{(n)} = \alpha^{(n-1)}\right\rangle , \tag{3}$$

where $\alpha^{(n)}$ and $\alpha^{(n-1)}$ are values of the conversion factor in two consecutive iterations and n is the iteration index. After substituting $\alpha^{(n)}$ (instead of α_{opt}) and $\boldsymbol{C}_{mf}$ given by Eq. (3) into Eq. (2), the latter could be resolved analytically. In this study, the first iteration (based on the initial model run) was performed with the reference value of the conversion factor, α_r (see Sect. 2.1.2). Three iterations were found to be sufficient in order to ensure that $\alpha^{(n)}$ is converged to the optimal estimate of α with the relative numerical uncertainty of less than 5 %.

Confidence intervals for α_{opt} were evaluated by means of a Monte Carlo experiment based on the bootstrapping method [41]. Specifically, the simulations performed with the optimal value of α were used to represent the "true" values of the BB fraction of the tropospheric NO_2 columns. The corresponding "observed" values were generated by sampling random errors from the residuals of the modeled (optimal) data for NO_2 columns (see the right-hand part of Eq. (2)) and adding them to such "true" values. The re-sampling procedure and estimation of α_{opt} (assuming a linear dependence of $\boldsymbol{C}_{mf}$ on α) were repeated 1000 times. The confidence intervals were evaluated (and are reported below) in terms of the 95th percentile.

Since the tropospheric NO_2 columns derived from satellite measurements provide information only on NO_x emissions, there is an issue concerning specification of BB emissions of other species (such as CO and volatile organic compounds, VOCs). As the main option, we used the same values of the conversion factor to calculate the BB emissions of all model species. This estimation case is labeled below as "VOCbyNO$_x$". However, as it was pointed out earlier [21, 36], estimates of α derived from measurements of different species may be different, partly due to uncertainties in the assumed emission factors. Therefore, as another option, we calculated the BB emissions of CO and VOCs by using the value of α optimized in a previous study [21] against ground-based measurements of CO concentrations in the Moscow region: such a CO-measurement-based value of α had been found to be a factor of 1.88 larger than its reference value α_r. The second estimation case is labeled below as "VOCbyCO".

Note that the estimation method described above is similar but not identical to those employed in the preceding studies [21, 36] where satellite measurements and the CHIMERE model were used to constrain emissions of CO and aerosol from wildfires in Russia. The differences (that will not be discussed here in detail) are mainly due to the fact that CO and aerosol are much less reactive species compared to NO_x. Some specific assumptions (for example, those concerning character of possible systematic uncertainties in simulated data) involved in the preceding studies are no longer valid in the case considered in this study and should have been avoided. Consequently, estimation of BB NO_x emissions using exactly the same methods as those employed in the previous studies turned out to be infeasible, and so such methods had to be modified accordingly.

To study a potential impact of chemical nonlinearities on BB NO_x emission estimates based on satellite measurements, we performed several additional model runs using BB emissions calculated with different values of the conversion factor. Specifically, the reference value of the conversion factor was scaled with a factor ranging from 0. 5 to 2, and the resulting values were used in Eq. (3) as the "zero-order" estimate, $\alpha^{(0)}$, to obtain the "first-order" estimate (constrained by satellite measurements) of the conversion factor, $\alpha^{(1)}$. Furthermore, we estimated the effective lifetime of NO_x, τ_{NO_x}, corresponding to each value of $\alpha^{(0)}$ as follows:

$$\tau_{nox} = \left(\sum_{i=1}^{Nd} \sum_{j=1}^{Nc} \theta^{ij} e^{ij} \right)^{-1} \sum_{i=1}^{Nd} \sum_{j=1}^{Nc} \theta^{ij} v^{ij} , \tag{4}$$

where e^{ij} are the BB NO_x emission rates (g hour^{-1}) in a grid cell j and in a day i, v^{ij} are values (simulated by the CHIMERE model) of the tropospheric column amounts of NO_x originating from wildfires, N_c and N_d are the total numbers of grid cell and days in the study region and period, and θ^{ij} is the selection operator which is equal to unity if the measurement data for a given grid cell and day is available and zero otherwise. Eq. (4) assumes that the evolution of the total (integral) amount of NO_x from BB burning over the study region can be roughly approximated by a simple balance

equation describing the loss of NO_x as a first order decay process, with the rate expressed as τ_{NOx}^{-1}. It also assumes that that BB NO_x emissions and NO_x column amounts are in an instantaneous balance. Similar assumptions were made in the previous studies [12-14] mentioned above. Note that the relationship between $\alpha^{(1)}$ and $\alpha^{(0)}$ depends not only on the NO_x lifetime but also on the of NO_2 / NO ratio: this ratio, in turn, depends on ozone concentration and can be affected by changes in the NO_x emissions. In addition, unlike τ_{NOx} calculated using Eq. (4), estimation of $\alpha^{(1)}$ partly takes into account BB NO_x emissions in grid cells (days) for which the measurement data are not available. Therefore, the dependence of τ_{NOx} on $\alpha^{(0)}$ cannot fully characterize that of the NO_2 columns retrieved from OMI measurements on the BB NO_x emission rate in the study region and period. Nonetheless, we believe that the estimates of τ_{NOx} provided below can be helpful in characterizing the processes determining the relationship between the NO_2 columns and NO_x emissions. Furthermore, such estimates obtained in different ways can eventually contribute to reducing uncertainties associated with FER or EC estimates [7, 11-14] based on the analysis of the empirical relationships between FRP and tropospheric NO_2 columns.

3. Results

3.1. Estimation of the FRP-to-BBR conversion factor

Estimation of the conversion factor (as explained in the previous section) is based on the analysis of daily time series of spatially averaged NO_2 columns derived from the OMI measurements (C_o) and simulated with the CHIMERE model (C_{mf}) and involves evaluation of the background fraction (C_b) of the tropospheric NO_2 columns. The corresponding time series are presented in Figure 1, along with the time series of the difference of C_o and C_b. Examples of underlying daily values of tropospheric NO_2 columns (specifically, on 29 July and 8 August) spatially distributed inside of the study region are shown in Figure 2. Note that values of C_{mf} shown in Figure 1 and Figure 2 were calculated with the conversion factor equal to its reference value α_r specified above (see Sect. 2.1.2). Note also that the spatial distributions CO and aerosol on the same days were considered in a preceding study [21].
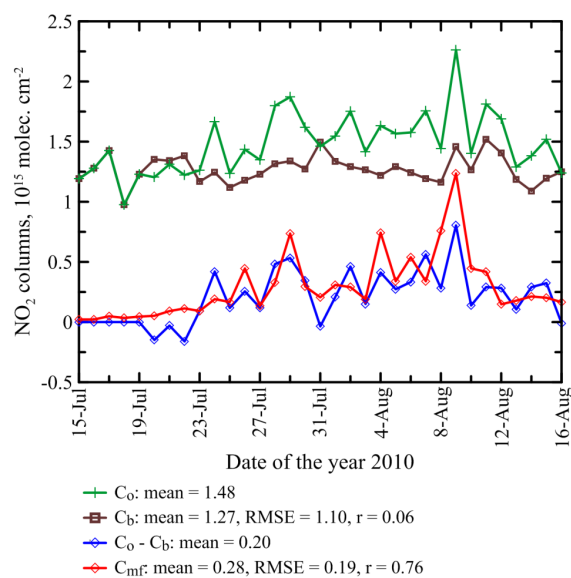

Figure 1. Time series of the daily NO_2 column amounts averaged over the study region. C_o: the tropospheric NO_2 columns retrieved from OMI measurements; C_b: a background part of tropospheric NO_2 columns; C_{mf}: the simulated tropospheric column amounts of NO_2 from wildfires. The RMSE and the correlation coefficient indicated in the figure legend for C_b and C_{mf} were calculated relative to C_o and $C_o - C_b$, respectively.

As it evident from Figure 1, the simulations tend to overestimate the BB part (that is the difference of C_o and C_b) of NO_2 columns, although the model captures, to a significant extent, the temporal variability of NO_2 column amounts from wildfires (specifically, the correlation coefficient exceeds a value of 0.75). The fact that, for some days, C_b is larger than C_o indicates that there may be considerable uncertainties in our estimates of background NO_2 values as well as in the original satellite NO_2 data. We expect that such uncertainties are mostly random in nature (varying from day to day) and are thus taken into account in the confidence intervals of our emission estimates reported below.
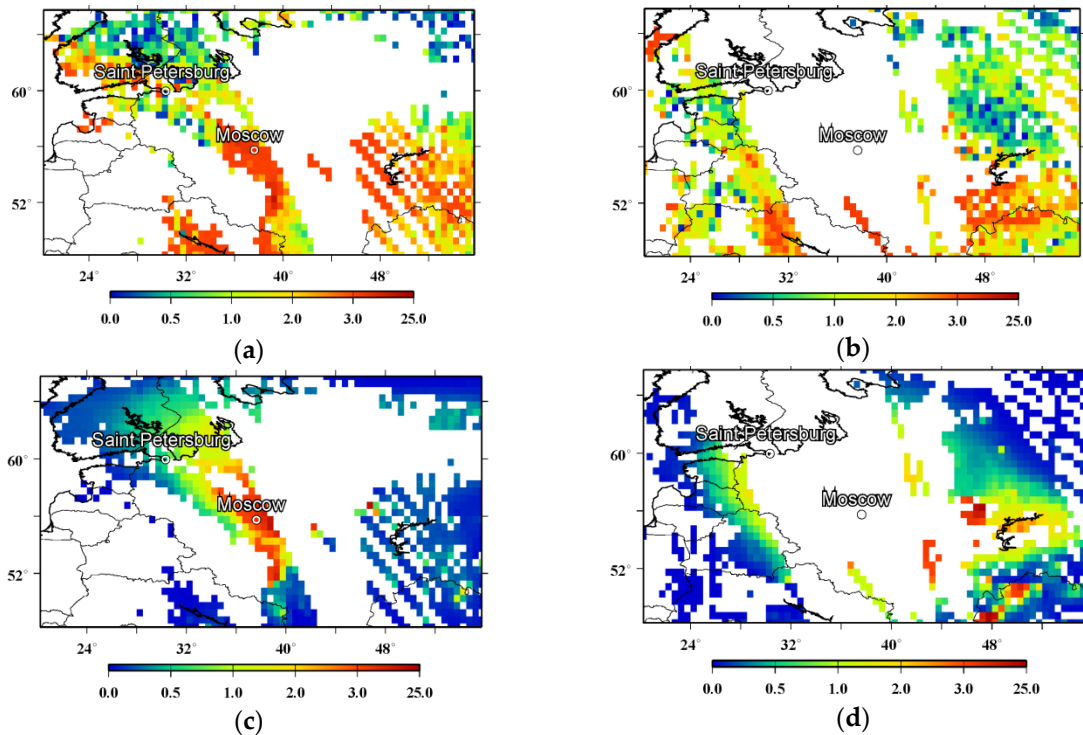
Figure 2. (a,b) Spatial distributions of the tropospheric NO_2 columns derived from the OMI measurements on 29 July and 8 August 2010; **(c,d)** tropospheric column amounts of NO_2 originating from wildfires, according to the simulations using the reference value of the FRP-to-BBR conversion factor. Note that the simulation data were processed with the averaging kernels from the OMI retrievals, so they are missing whereas the measurement data were unavailable.

Examples of spatial distributions of NO_2 columns shown in Figure 2 illustrate the fact that NO_2 retrievals for many scenes in the study region and period were missing (apparently, due to interference of BB aerosol that is "shielding" radiation from the boundary layer). Nonetheless, many moderately polluted scenes where, according to our simulations, considerable amounts of NO_2 originated from wildfires can still be seen in the OMI retrievals.

Figure 3 presents the conversion factor estimates, $\alpha^{(n)}$, that were obtained according to Eq. (2) and (3) by using the simulations in which BB emissions were calculated with the assumed conversion factor values, $\alpha^{(n-1)}$. For convenience, values of both $\alpha^{(n)}$ and $\alpha^{(n-1)}$ are normalized to the reference value of the conversion factor, α_r. Most of the estimates shown in Figure 3 illustrate results of the first iteration (n=1), except for the optimal estimates (circumvented by black circles in Figure 3) of α (α_{opt}) that were obtained as a result of the third iteration (n=3). The estimates were obtained separately for the two cases ("VOCbyNO$_x$" and "VOCbyCO") that involve different assumptions regarding the BB emissions of VOCs and CO. If the relationship between the simulated NO_2 columns and BB NO_x emissions were linear, then any value of $\alpha^{(n-1)}$ would yield a unique value of $\alpha^{(n)}$, or, in other words, $\alpha^{(n)}$ would be independent on $\alpha^{(n-1)}$. Our results show that $\alpha^{(n)}$ is indeed very weakly (positively) dependent on $\alpha^{(n-1)}$ for the case "VOCbyNO$_x$", while a more pronounced decreasing

dependence of $\alpha^{(n)}$ on $\alpha^{(n-1)}$ is found for the case "VOCbyCO". Overall, our results shown in Figure 3 indicate that the effects of chemical nonlinearities on the relationship between the BB emissions and tropospheric NO_2 columns in the situation considered cannot be disregarded without constraints on VOCs emissions, although such effects are not very strong. In particular, the increase of $\alpha^{(0)}$ from 0.5 to 2 (that is, by a factor 4) in the "VOCbyCO" case resulted in the decrease of $\alpha^{(1)}$ from 0.96 to 0.67 (that is, by only about 30 percent). Note that the decrease of $\alpha^{(1)}$ is a manifestation of the corresponding increase (by a factor of ~ 1.3) of the ratio of the mean BB NO_2 column amounts and NO_x emission rates in the respective simulations. It is especially noteworthy that the sensitivity of the optimal estimates of α_r to changes in BB VOC emissions turned out to relatively small: specifically, while BB VOCs emissions for the "VOCbyCO" case were almost a factor of 3 larger than for the "VOCbyNO$_x$" case (when $\alpha=\alpha_{opt}$), the optimal estimate of the conversion factor is found to be only 17 percent larger for the former case (0.298 ± 0.053 kg s^{-1} MW^{-1}) than that for the latter one (0.254 ± 0.045 kg s^{-1} MW^{-1}). Unfortunately, there are presently no data that would allow us to characterize the uncertainty of the regionally averaged emission factors for VOCs, although such uncertainty is likely much smaller than the standard deviation (close to 100 % [42]) of individual emission factor measurements. Note that systematic uncertainties in our estimates of α due to biases in the emission factors for VOCs are probably only partly accounted for in the confidence intervals for the respective estimates, to an extent as such uncertainties are associated with errors in the simulated daily variations of the tropospheric NO_2 columns.
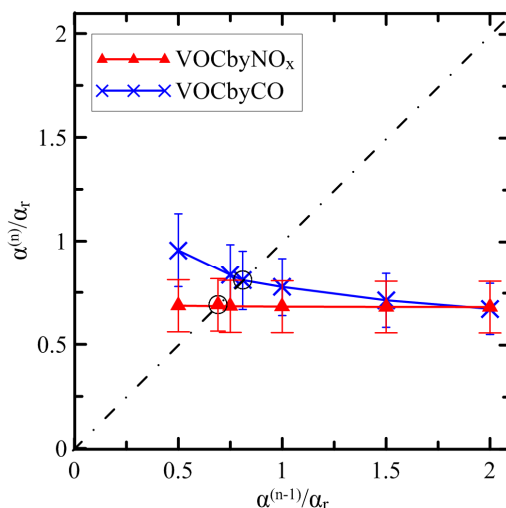

Figure 3. Dependence of the FRP-to-BBR conversion factor values optimized under the assumption of linearity of the relationship between the NO_2 columns and the BB NO_x emission rate on an assumed value of the same conversion factor. The conversion factor values are normalized to their reference value. The dependence is shown for the two estimation cases, "VOCbyNO$_x$" and "VOCbyCO", see Sect. 2.2. The estimates circumvented by black circles are the optimal estimates (α_{opt}) obtained as a result of third iteration (that is, with n=3) of the iterative procedure described in Sect. 2.2, whereas the other estimates are a result of an initial iteration (n=1).

Another potential source for a bias in our emission estimates is due to uncertainties in estimates of the background estimates of the NO_2 columns. To test the sensitivity of our results to this factor, we repeated our estimation procedure for the VOCbyNO$_x$ case, but with the background NO_2 columns estimated using available observational data for other days (12 - 14 July 2010 instead of 15-19 July 2010 as in the base case). The optimal estimate of α for the test case was found to be only 10 percent larger than for the base case. This result indicates that our BB NO_x emission estimates are sufficiently robust with regard to random uncertainties in the background NO_2 column amounts. Furthermore, we investigated whether or not the background NO_2 columns changed significantly over the study period (due to, e.g., changes in meteorological conditions or in biogenic emission

rates). To this end, we selected data points (grid cells and days) where the simulated NO_2 column amounts originating from fires were infinitesimal (less than 10^{-2} %), relatively to the background NO_2 columns estimated for the same grid cells / days using the OMI data for the period 15-19 July 2010. The selected data were averaged separately over the periods 15-19 July 2010 and 20 July-16 August 2010. As a result, the mean value over the second period was found to be very insignificantly (~ 6 %) lower than that for the first period. This result confirms that uncertainties in our estimates of α due to uncertainties associated with evaluation of the background NO_2 columns are unlikely to exceed the statistical uncertainties represented by the confidence intervals for the values of α_{opt}.
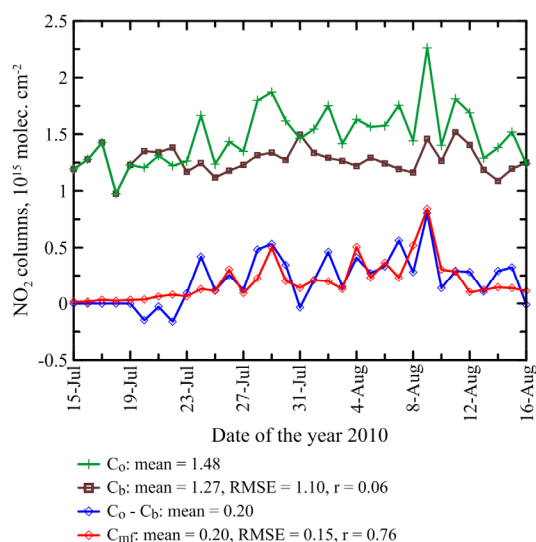

Figure 4. The same as in Figure 1, except that the simulated time series, C_{mf}, were obtained from the model run using the optimal value of the FRP-to-BBR conversion factor for the VOCbyNO$_x$ case.

Figure 4 illustrates the performance of our NO_2 simulation using optimized NO_x emissions for the VOCbyNO$_x$ case. Note that the simulation data for the VOCbyCO case are almost indistinguishable from those in the VOCbyNO$_x$ case and are not presented here. The daily time series shown in Figure 4 are the same as those in Figure 1, except that the BB NO_x emissions used in the simulation presented in Figure 5 were calculated with the optimal estimate of α (α_{opt}) instead of its reference value (α_r) as in Figure 1. Evidently, compared to the model results obtained with the reference value of α, the performance of the "optimal" simulation is noticeably better. Specifically, the root mean square error (RMSE) has reduced by more than 20 % and a considerable difference (~ 40 %) between the mean values of the NO_2 columns from the model and measurements has practically been eliminated. It is noteworthy that the optimization of the NO_x BB emissions did not affect a value of the correlation coefficient (r). This observation implies that the correlation coefficient in the given case can be considered as an independent (of α) measure of accuracy of the spatial-temporal field of the BB NO_x emissions used in our simulations.

The spatial distributions of the average (over the study period) NO_2 column amounts obtained using the OMI measurements and given by the CHIMERE model run are compared in Figure 5(a, b). For the comparison purpose, the simulated BB NO_2 column amounts (C_{mf}) were added to the background values of the NO_2 columns (C_b). Evidently, such "composed" data demonstrate a rather reasonable, although not perfect, agreement with the measurement data. This kind of agreement provides one more argument for reliability of our estimation procedure. Note that, in accordance to our results shown in Figure 4, a contribution of fires to the tropospheric NO_2 columns is found to be relatively small (see Figure 5c).
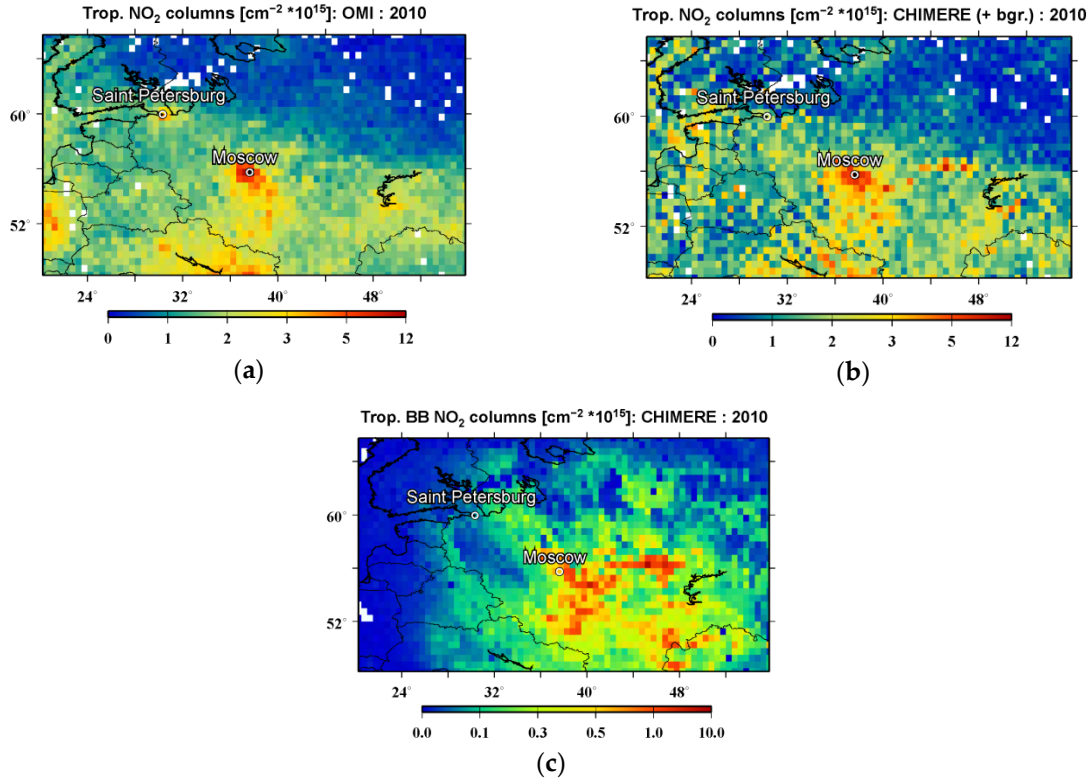
3.2 NO$_x$ lifetime estimates

(a)

(b)

(c)

Figure 5. The spatial distributions of the average (over the study period) NO_2 column amounts obtained using the OMI measurements (**a**) and the modeled data that were composed by summing up the simulated tropospheric column amounts of NO_2 from fires and the background values of the tropospheric NO_2 columns (**b**). The simulated tropospheric column amounts of NO_2 from fires are also shown separately (**c**).
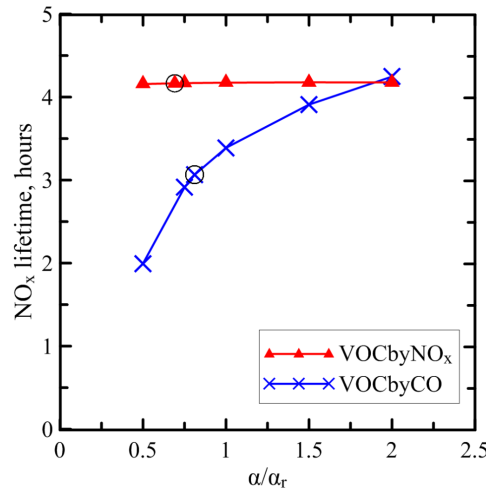

Figure 6. The effective NO_x lifetime (τ_{NO_x}) estimated a function of the FRP-to-BBR conversion factor (α) normalized to its reference value (α_r). Black circles depict the NO_x lifetime values corresponding to the optimal estimates of α for the two estimation cases ("VOCbyNO$_x$" and "VOCbyCO") considered in this study.

The NO_x lifetime estimates (τ_{NO_x}) obtained in accordance to Eq. (4) are presented in Figure 6 as a function of α for the two estimation cases ("VOCbyNO$_x$" and "VOCbyCO"). Similar to the dependencies of $\alpha^{(n)}$ on $\alpha^{(n-1)}$ that are shown in Figure 3, the dependencies of τ_{NO_x} on α for the two cases are qualitatively different. Specifically, while the case "VOCbyNO$_x$" features almost constant

NO_x lifetimes irrespectively of the assumed values of the conversion factor, the values of τ_{NOx} obtained for the "VOCbyCO" case are increasing by a factor of 2.1 with the increase of α by a factor of 4. The NO_x lifetime values corresponding to the optimal estimates of the conversion factor are 4.2 and 3.1 hours for the "VOCbyNO$_x$" and "VOCbyCO" cases. These values are within of a rather broad range of lifetimes (2 ÷ 6 hours) assumed in earlier studies of BB NO_x emissions [11-14]. Importantly, the relative difference between the lifetimes calculated for the "VOCbyNO$_x$" and "VOCbyCO" cases is much larger compared to the relative difference between values of α_{opt} (see Figure 3) for the same cases: this fact indicates that the difference of the lifetimes is counterbalanced by the difference of the NO_2 / NO ratio.

Exhaustive theoretical interpretation of the dependencies shown in Figure 6 goes beyond the scope of this study. Here, we discuss the chemical mechanisms underlying these dependencies only very briefly. In particular, we note that NO_x is mainly removed from the atmosphere in a reaction of NO_2 with OH [1]. Both OH and NO_2 concentrations are typically growing functions of ozone (O_3) concentration [1]. Our simulation data for O_3 and OH concentrations (not presented here) indicate that "hot spots" featuring strong BB emissions typically coincide in space and time with depleted concentrations of these species, as well as with reduced values of NO_2 / NO ratio. It can be speculated that the behavior of the O_3 formation rate is the main factor determining a nearly linear dependence of NO_2 concentration on the BB NO_x emission rate in the indicated case. Specifically, in the "high NO_x limit" (in which OH concentration is relatively small), the O_3 formation rate is known to be proportional to the ratio of VOC to NO_x concentrations [1] and thus can be expected to be independent on α in the "VOCbyNO$_x$" case. In contrast, the VOC emission rate is independent on α in the "VOCbyCO" case. Thus the O_3 formation rate is likely to decrease with an increase of α, leading to the observed increase in the NO_x lifetime.

Such an interpretation of the results presented in Figure 6 is consistent with the dependencies presented in Figure 3. Indeed, given that the NO_x lifetime is almost independent on α in the "VOCbyNO$_x$", the results shown in Figure 3 for the same case imply that the NO_2 / NO ratio and thus O_3 concentration are also kept nearly constant. On the other hand, the fact that the relative range of the changes of $\alpha^{(n)}$ in the "VOCbyCO" case in Figure 3 is much smaller than that of the changes of τ_{NOx} in Figure 6 indicates that the NO_2 / NO ratio decreases with an increase of α in that case: this observation, in turn, implies that O_3 concentration accordingly decreases.

3.3. NO$_x$ emission estimates

We used our optimal estimate of the FRP-to-BBR conversion factor (0.254 kg s^{-1} MW^{-1}) for the VOCbyNO$_x$ case to calculate NO_x emission rates from wildfires in the study region and period. Figure 7 shows time series of daily BB NO_x emission rates that were obtained by integrating either over all grid cells and hours of a given day or only over selected grid cells / hours that were provided with the OMI NO_2 data. According to our calculations, the "full" emissions tended to increase until 6 August and then started to decrease, consistently with results of other studies [9,19,21,43] that reported on the strong air pollution in the study region in the beginning of August. Two major peaks of the BB NO_x emission rate occurred on August 4 and 6. A difference between the two time series indicates to what extent the information provided by the OMI retrievals on BB NO_x emissions is representative of the whole study period. Evidently, the BB NO_x emission rates corresponding to the scenes provided with the OMI NO_2 retrievals represent only a part (around 30 %, on the average) of integral emission rates in the study region and period. Therefore, there is a question whether or not our optimal estimate of the FRP-to-BBR conversion factor is representative (at least, on average) of all fires in the study region.

Figure 8 presents spatial distributions of the BB NO_x emission rates averaged over the study period. The two different distributions (shown in Figure 8a and 8b) correspond to the two respective time series presented in Figure 7. Expectedly, the distribution obtained only with the selected data typically features smaller BB NO_x emission rates compared to the one obtained using all the available emission data. Nonetheless, it is important to note that both the coverage and spatial structure of the emission rates shown in the different distributions are rather similar. Therefore, a comparison of the spatial distributions shown in Figure 8a and 8b provides evidence

that our optimal conversion factor estimate that was used to scale BB NO$_x$ emissions rates across the study region is sufficiently representative of the whole region and period considered. Note that a special test involving splitting the study period into two approximately equal parts has shown that the difference between the optimal values of the conversion factor for those periods was less than the statistical uncertainty of our estimate for the whole period. Although a result of such a test provides further evidence in favor of applicability of our optimal conversion factor estimates across the study region and period, the question regarding the representativeness of the conversion factor estimates derived from observations of limited number of fire scenes still remains and requires further investigations that go beyond of the scope of this study.
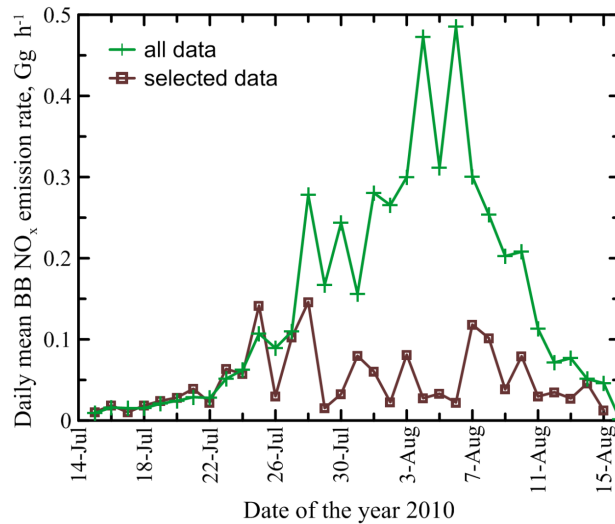

Figure 7. Time series of the daily mean BB NO$_x$ emission rates that were obtained by integrating either over all model grid cells (see a green curve) or only over selected grid cells that are provided with the OMI NO$_2$ data for a given day (see a brown curve).
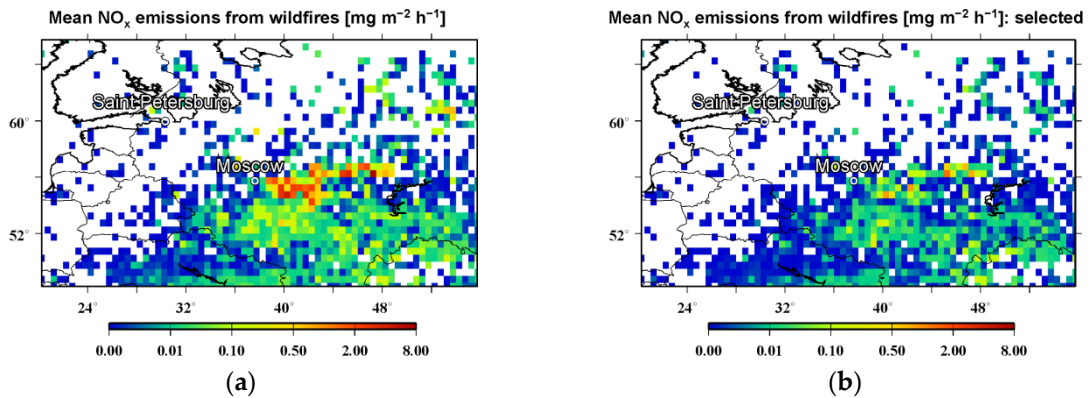

Figure 8. Spatial distributions of the BB NO$_x$ emission rates averaged over the study period. The two different distributions are obtained by averaging either over all model grid cells and hours in the study period (a) or only those grid cells / hours which are provided with the OMI NO$_2$ retrievals (b) and correspond to the green and brown curves in Fig. 7, respectively.

Figure 9 compares our estimates of the total BB NO$_x$ emissions in the study region and period with corresponding estimates obtained using the data of "bottom-up" emission inventories, such as GFED4.1s [8] and GFAS v1.0 [9]. The GFED inventory is based on satellite measurements of burned area and other parameters from a biosphere model, while the GFAS inventory infers BB emissions from the FRP satellite measurements by using a method similar to one employed in this study. However, unlike our method, where the conversion factor is optimized against atmospheric composition measurements, the GFAS inventory uses conversion factor values calibrated with the

GFED data. Thus the GFED4.1s and GFAS v1.0 inventories are not fully independent, although the spatial structure and temporal variability of regional emission fields provided by these inventories may be significantly different. Our results suggest that both GFED4.1 and GFAS v1.0 considerably (by factors of 1.50 and 1.44, respectively) underestimate BB NO_x emissions and that the difference between our emission estimate and the respective inventory data cannot be explained by statistical uncertainties in our estimate. This finding is qualitatively consistent with results of other studies (see, e.g., [19-21, 36]) where those inventories were found to underestimate emissions of other species (such as CO and aerosol) from wildfires in Russia. It should be kept in mind, however, that the confidence intervals shown in Figure 9 may not fully account for possible biases in our estimates due to several factors mentioned above, including uncertainties in the VOC BB emissions and in background NO_2 column amounts, probable negative biases in satellite NO_2 retrievals for the strongly polluted scenes, as well as possibly insufficient spatial and temporal representativeness of the observational constraints provided by the available NO_2 satellite measurements to BB NO_x emissions. Quantitative understanding of these factors and their impacts on BB NO_x emission estimates inferred from satellite NO_2 measurements calls for further dedicated studies.
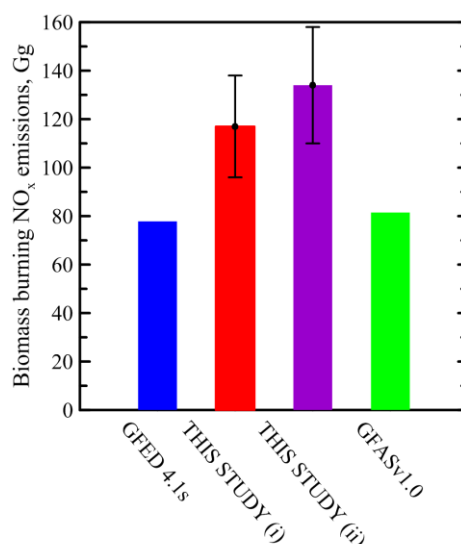

Figure 9. Optimal estimates of the total NO_x emissions in the study region and period in comparison with corresponding estimates based on data of the GFED4.1s and GFASv1.0 emission inventories. The optimal estimates are shown separately for the two estimation cases, "VOCbyNO$_x$" (*i*) and "VOCbyCO" (*ii*). The confidence intervals represent statistical uncertainty evaluated in terms of the 95th percentile.

4. Conclusions

In this paper, we examined feasibility of estimating NO_x emissions from wildfires within an inverse modeling approach by using satellite measurements of NO_2 columns. For this purpose, we considered the situation of the mega-fire event that occurred in the European part of Russia in July – August 2010. We used tropospheric NO_2 columns available from satellite measurements performed with the OMI instrument along with NO_2 column amounts simulated with the CHIMERE chemistry transport model (CTM) where emissions of NO_x and other species from biomass burning (BB) were taken into account. The BB emissions were calculated using the Fire Radiative Power (FRP) data that were available from satellite measurements with the MODIS instrument. The measured and simulated NO_2 columns were combined in the framework of a simple inverse modeling method aimed at estimating the conversion factor (α) from FRP to BB rate. Given an estimate of α, BB emissions of individual model species were calculated using typical emission factors reported in literature.

The focus in our study was given to analysis of the effect of chemical nonlinearities on the relationship between BB NO_x emissions and respective NO_2 column amounts. While in our study this relationship was simulated with CTM, several previous studies (mentioned in the Introduction) where BB NO_x emissions were investigated using NO_2 OMI measurements, involved explicit quantitative assumptions regarding the dependence of NO_2 columns on BB NO_x emissions. To test robustness of such assumptions, we performed several model runs where a typical "reference" value of the conversion factor (and thus the mean BB NO_x emission rate) was scaled with a factor ranging from 0.5 to 2.0. The simulations were done for the two cases involving different assumptions regarding emissions of volatile organic compounds (VOCs) and CO. Specifically, in one of the cases ("VOCbyNO$_x$"), VOCs and CO emission rates were scaled in the same way as the NO_x emissions, while in another case ("VOCbyCO"), the VOCs and CO emission rates were calculated with the α value inferred in a previous study from CO ground-based measurements and were kept constant irrespectively of changes of the NO_x emission rates. The corresponding linearized relationships (predicted by the model) between the NO_2 columns and BB NO_x emission rate were used to obtain optimal estimates of α. Furthermore, using results of the same model runs, we evaluated the effective NO_x lifetime.

It is found that the available measurement data and simulations yield a reasonable estimate of the conversion factor with a statistical uncertainty (evaluated in terms of the 95th percentile) of about ± 20 %. The optimal value of the conversion factor for the VOCbyNO$_x$ case is estimated to be ~0.25 kg s^{-1} MW^{-1}. This value is about 30 % smaller than the respective "reference" estimate (of 0.368 kg s^{-1}) obtained earlier in a laboratory experiment. The optimal estimate for the VOCbyCO case is found to be about 15 % larger compared to the estimate for the VOCbyNO$_x$ case. Note that the differences between our and reference estimates of the conversion factor may, in principle, compensate for a biases in the NO_x emission factors specified in our simulations, since our emission model involves a multiplicative combination of the both factors.

Our results indicate that chemical nonlinearities may have considerably different effects on the relationship between BB NO_x emissions and NO_2 columns, depending on an assumed ratio of the NO_x and VOC emission rates. Specifically, in the VOCbyNO$_x$ case, where that ratio was kept constant, both the NO_2 columns-NO_x emissions relationship and the effective NO_x lifetime were found to be almost independent upon variations of an assumed value of the conversion factor α. The effective NO_x lifetime for this case was estimated to be ~ 4.2 h which is within a broad range of NO_x lifetimes (2÷6 h) assumed in previous studies [11-14]. In contrast, in the VOCbyCO case, both the BB NO_2 columns / BB NO_x emission rate ratio and the effective NO_x lifetime were found to substantially increase with an increase of the NO_x emission rate (scaled uniformly with α). In particular, the effective NO_x lifetime is found to increase from ~ 2.0 to 4.2 h as the conversion factor used in our simulations increased from 0.184 to 0.736 kg s^{-1} MW^{-1}. These results imply that in a common case where the BB VOC emission rates are not constrained by respective measurements, the NO_x lifetime (as well as the relationship between the NO_2 columns and BB NO_x emission rates) remains, to some extent, uncertain and the effects of chemical nonlinearities on BB NOx emission estimates should not "a priori" disregarded.

The optimized values of the conversion factors were used to estimate the total NO_x amount emitted from wildfires in the study region in the period from 15 July to 16 August. Our estimates are found to be at least a factor of 1.4 larger compared to the corresponding values predicted by the GFED4.1 and GFASv1.0 fire emission inventories. The differences between our estimates and the inventory data considerably exceed the statistical confidence intervals of our estimates. This result suggests that both of the inventories are likely to underestimate NO_x emissions from the Russian 2010 wildfires. However, it should be noted that the statistical confidence intervals for our emission estimates do not necessarily account for all kinds of systematic uncertainties in measurement and simulation data used in our analysis. Such uncertainties may include those in the BB VOC emissions, in background NO_2 column amounts, probable negative biases in satellite NO_2 retrievals for the strongly polluted scenes, as well as biases due to limited spatial and temporal coverage of

available NO_2 satellite measurements. Evaluation of these uncertainties goes beyond the scope of this study and should be addressed in future studies. Nonetheless, even in view of the probable uncertainties, we believe that our independent BB NO_x emission estimates constrained by satellite measurements are a useful contribution to a practically important research direction dealing with evaluation of BB emissions, especially taking into account that available fire emission data provided by "bottom-up" inventories may also be subject to various poorly known uncertainties.

Author Contributions: E.V.B. performed simulations and created computer programs used in the analysis. I.B.K. conceived the method of the analysis and wrote the paper, Y.Y.R contributed to the analysis of the simulation and measurement data and to technical preparation of the paper.

Conflicts of Interest: The authors declare no conflict of interest. The founding sponsors had no role in the design of the study; in the collection, analyses, or interpretation of data; in the writing of the manuscript, and in the decision to publish the results.

Abbreviations

The following abbreviations are used in this manuscript:

BB: Biomass burning
BBR: Biomass burning rate
CTM: Chemistry transport model
EC: emission coefficient
FER: Fire emission rate
FRP : Fire radiative power
KNMI: The Royal Netherland Meteorological Institute
MODIS: The Moderate Resolution Imaging Spectroradiometer
OMI: Ozone monitoring instrument
RMSE: Root mean square error
VOCs: Volatile organic compounds

References

1. Seinfeld, J.H.; Pandis, S.N. Chemistry of the troposphere. In *Atmospheric chemistry and physics: From air pollution to climate change,* 2nd Ed. Wiley-Interscience, J. Wiley & Sons, Inc: New York, USA, 2006; pp. 204-230.
2. Monks, P.S. Gas-phase radical chemistry in the troposphere. *Chem. Soc. Rev.* **2005**, *34*, 376-395, DOI: 10.1039/b307982c.
3. Konovalov, I.B. Nonlinear relationships between atmospheric aerosol and its gaseous precursors: Analysis of long-term air quality monitoring data by means of neural networks. *Atmos. Chem. Phys.* **2003**, 607-621, DOI:10.5194/acp-3-607-2003.
4. Ng, N.L.; Chhabra, P.S., Chan; A.W.H.; Surratt, J.D.; Kroll, J.H.; Kwan, A.J.; McCabe, D.C.; Wennberg, P.O.; Sorooshian, A.; Murphy, S.M.; Dalleska, N.F.; Flagan, R.C.; Seinfeld, J. H. Effect of NO_x level on secondary organic aerosol (SOA) formation from the photooxidation of terpenes. *Atmos. Chem. Phys.* **2007**, *7*, 5159-5174, DOI:10.5194/acp-7-5159-2007.
5. Denman, K.L.; Brasseur, A.; Chidthaisong, A.; Ciais, P.; Cox, P.M.; Dickinson, R.E.; Hauglustaine, D.; Heinze, C.; Holland, E.; Jacob, D.; Lohmann, U.; Ramachandran, S.; da Silva Dias, P.L.; Wofsy, S.C.; Zhang, X. Couplings Between Changes in the Climate System and Biogeochemistry, In: *Climate Change 2007: The Physical Science Basis, Contribution of Working Group I to the Fourth Assessment Report of the Intergovernmental Panel on Climate Change,* Solomon, S., Qin, D., Manning, M., Chen, Z., Marquis, M.,

Averyt, K. B., Tignor, M., and Miller, H. L., Eds.; Publisher: Cambridge University Press, Cambridge, UK and New York, NY, USA, 2007, pp. 499–588.

6.   Jaffe, D.A.; Wigder, N.L. Ozone production from wildfires: A critical review. *Atmos. Environ* **2012,** *51,* 1–10, DOI:10.1016/j.atmosenv.2011.11.063.

7.   Mebust, A.K.; Russell, A.R.; Hudman, R.C.; Valin, L.C.; Cohen, R.C. Characterization of wildfire NO_x emissions using MODIS fire radiative power and OMI tropospheric NO_2 columns, *Atmos. Chem. Phys.* **2012**, *11*, 5839-5851, DOI:10.5194/acp-11-5839-2011.

8.   Randerson, J.T.; van der Werf, G.R.; Giglio, L; Collatz, G.J.; Kasibhatla, P.S. 2015, Global Fire Emissions Database, Version 4, (GFEDv4). ORNL DAAC, Oak Ridge, Tennessee, USA. Available online: http://dx.doi.org/10.3334/ORNLDAAC/1293.

9.   Kaiser, J.W.; Heil, A.; Andreae, M.O.; Benedetti, A.; Chubarova, N.; Jones, L.; Morcrette, J.-J.; Razinger, M.; Schultz, M.G.; Suttie, M.; van der Werf, G. R. Biomass burning emissions estimated with a global fire assimilation system based on observed fire radiative power. *Biogeosciences* **2012**, *9*, 527–554, DOI:10.5194/bg-9-527-2012.

10. Akagi, S. K.; Yokelson, R. J.; Wiedinmyer, C.; Alvarado, M. J.; Reid, J. S.; Karl, T.; Crounse, J. D.; and Wennberg, P. O. Emission factors for open and domestic biomass burning for use in atmospheric models, *Atmos. Chem. Phys.*, **2011**, 11, 4039-4072, doi:10.5194/acp-11-4039-2011.

11. Mebust, A.K.; Cohen, R.C. Space-based observations of fire NO_x emission coefficients: a global biome-scale comparison. *Atmos. Chem. Phys.* **2014**, *14*, 2509-2524, DOI:10.5194/acp-14-2509-2014.

12. Schreier, S.F.; Richter, A.; Kaiser, J.W.; Burrows, J. P. The empirical relationship between satellite-derived tropospheric NO_2 and fire radiative power and possible implications for fire emission rates of NO_x. *Atmos. Chem. Phys.* **2014**, *14*, 2447-2466, DOI:10.5194/acp-14-2447-2014.

13. Tanimoto, H.K.; Ikeda, K.F.; Boersma, R.J.; van der Garivait, A.S. Interannual variability of nitrogen oxides emissions from boreal fires in Siberia and Alaska during 1996–2011 as observed from space. *Environ. Res. Lett.* **2015**, *10*, 065004, DOI:10.1088/1748-9326/10/6/065004.

14. Schreier, S.F.; Richter, A.; Schepaschenko, D.; Shvidenko, A.; Hilboll, A.; Burrows, J.P. Differences in satellite-derived NOx emission factors between Eurasian and North American boreal forest fires. *Atmos. Environ* **2015**, *121*, 55-65, DOI: 10.1016/j.atmosenv.2014.08.071.

15. Konovalov, I.B.; Beekmann, M.; Richter, A.; Burrows, J. P. Inverse modelling of the spatial distribution of NO_x emissions on a continental scale using satellite data. *Atmos. Chem. Phys.* **2006**, *6(7)*, 1747–1770, DOI:10.5194/acp-6-1747-2006.

16. Miyazaki, K.; Eskes, H.J.; Sudo, K. Global NO_x emission estimates derived from an assimilation of OMI tropospheric NO_2 columns. *Atmos Chem Phys* **2012**, *12(5)*, 2263–2288, DOI:10.5194/acp-12-2263-2012.

17. Mijling, B.; van der A, R.J. Using daily satellite observations to estimate emissions of short-lived air pollutants on a mesoscopic scale. *J. Geophys. Res.-Atmos.* **2012**, *117*, D17302, DOI:10.1029/2012JD017817.

18. Berezin, E.V.; Konovalov, I.B.; Ciais, P.; Richter, A.; Tao, S.; Janssens-Maenhout, G.; Beekmann, M.; Schulze, E.-D. Multiannual changes of CO_2 emissions in China: indirect estimates derived from satellite measurements of tropospheric NO_2 columns. *Atmos. Chem. Phys.* **2013**, *13(18)*, 9415–9438, DOI:10.5194/acp-13-9415-2013.

19. Konovalov, I.B.; Beekmann, M.; Kuznetsova, I.N.; Yurova, A.; Zvyagintsev, A.M. Atmospheric impacts of the 2010 Russian wildfires: integrating modelling and measurements of an extreme air pollution episode in the Moscow region. *Atmos. Chem. Phys.* **2011**, *11*, 10031–10056, DOI:10.5194/acp-11-10031-2011.

20. Krol, M.; Peters, W.; Hooghiemstra, P.; George, M.; Clerbaux, C.; Hurtmans, D.; McInerney, D.; Sedano, F.; Bergamaschi, P.; El Hajj, M.; Kaiser, J.W.; Fisher, D.; Yershov, V.; Muller, J.-P. How much CO was emitted by the 2010 fires around Moscow? *Atmos. Chem. Phys.* **2013**, *13*, 4737–4747, DOI:10.5194/acp-13-4737-2013.

21. Konovalov, I.B.; Beekmann, M.; Berezin, E.V.; Petetin, H.; Mielonen, T.; Kuznetsova, I.N.; Andreae, M. O. The role of semi-volatile organic compounds in the mesoscale evolution of biomass burning aerosol: a modeling case study of the 2010 mega-fire event in Russia. *Atmos. Chem. Phys.* **2015**, *15*, 13269-13297, doi:10.5194/acp-15-13269-2015.

22. Levelt, P.F.; Hilsenrath, E.; Leppelmeier, G.W.; van den Oord, G.H.J.; Bhartia, P.K.; Tamminen, J.; de Haan, J.F.; Veefkind, J.P. Science objectives of the ozone monitoring instrument. *IEEE Trans. Geosci. Remote Sens.* **2006**, *44*(5), 1199–1208, DOI:10.1109/TGRS.2006.872336.

23. Boersma, K.F.; Eskes, H.J.; Dirksen, R.J.; van der A, R.J.; Veefkind, J.P.; Stammes, P.; Huijnen, V.; Kleipool, Q.L.; Sneep, M.; Claas, J.; Leitão, J.; Richter, A.; Zhou, Y.; Brunner, D. An improved tropospheric NO_2 column retrieval algorithm for the Ozone Monitoring Instrument. *Atmos. Meas. Tech.* **2011**, *4*, 1905-1928, DOI:10.5194/amt-4-1905-2011.

24. TEMIS portal. Available online: http://www.temis.nl/ (accessed on 17 March 2016).

25. Irie, H.; Boersma, K.F.; Kanaya, Y.; Takashima, H.; Pan, X.; Wang, Z F. Quantitative bias estimates for tropospheric NO_2 columns retrieved from SCIAMACHY, OMI, and GOME-2 using a common standard for East Asia. *Atmos. Meas. Tech.* **2012**, *5*, 2403–2411, DOI:10.5194/amt-5-2403-2012.

26. Boersma, K.F.; Eskes, H.J.; Brinksma, E.J. Error analysis for tropospheric NO2 retrieval from space. *J. Geophys. Res.-Atmos.* **2004,** *109*, D04311, doi:10.1029/2003JD003962.

27. Kaufman, Y.J.; Justice, C.O.; Flynn, L.P.; Kendall, J.D.; Prins, E.M.; Giglio, L.; Ward, D.E.; Menzel, W.P.; Setzer, A.W. Potential global fire monitoring from EOS-MODIS. *J. Geophys. Res.* **1998**, *103*, 32215–32238.

28. Justice, C.O.; Giglio, L.; Korontzi, S.; Owens, J.; Morisette, J.T.; Roy, D.; Descloitres, J.; Alleaume, S.; Petitcolin, F.; Kaufman, Y. The MODIS fire products. *Remote Sens. Environ.* **2002**, *83*, 244–262.

29. The NASA Land Processes Distributed Active Archive Center. Available online: https://lpdaac.usgs.gov (accessed on 14 June 2015).

30. Remer, L.A.; Kaufman, Y.J.; Tanre, D.; Mattoo, S.; Chu, D.A.; Martins, J.V.; Li, R.-R.; Ichoku, C.; Levy, R.C.; Kleidman, R. G.; Eck, T. F.; Vermote, E.; Holben, B. N. The MODIS aerosol algorithm, products, and validation. *J. Atmos. Sci.* **2005**, *62*, 947–973.

31. The NASA Giovanni-Interactive Visualization and Analysis system. Available online: http://daac.gsfc.nasa.gov/giovanni/ (accessed on 23 June 2014).

32. Menut, L.; Bessagnet, B.; Khvorostyanov, D.; Beekmann, M.; Blond, N. Colette, A.; Coll, I.; Curci, G.; Foret, G.; Hodzic, A.; Mailler, S.; Meleux, F.; Monge, J.-L.; Pison, I.; Siour, G.; Turquety, S.; Valari, M.; Vautard, R.; Vivanco, M. G. CHIMERE 2013: a model for regional atmospheric composition modeling. *Geosci. Model Dev.* **2013**, *6*, 981–1028, DOI:10.5194/gmd-6-981-2013.

33. The CHIMERE chemistry-transport model. Available online: http://www.lmd.polytechnique.fr/chimere/ (accessed on 30 June 2016).

34. Hodzic, A.; Madronich, S.; Bohn, B.; Massie, S.; Menut, L.; Wiedinmyer, C. Wildfire particulate matter in Europe during summer 2003: meso-scale modeling of smoke emissions, transport and radiative effects. *Atmos. Chem. Phys.* **2007**, *7*, 4043–4064, DOI:10.5194/acp-7-4043-2007.

35. Konovalov, I. B.; Beekmann, M.; D'Anna, B.; George, C. Significant light induced ozone loss on biomass burning aerosol: Evidence from chemistry-transport modeling based on new laboratory studies. *Geophys. Res. Lett.* **2012**, *39*, DOI:10.1029/2012GL052432.

36. Konovalov, I.B.; Berezin, E.V.; Ciais, P.; Broquet, G.; Beekmann, M.; Hadji-Lazaro, J.; Clerbaux, C.; Andreae, M.O.; Kaiser, J.W.; Schulze, E.-D. Constraining CO_2 emissions from open biomass burning by satellite observations of co-emitted species: a method and its application to wildfires in Siberia. *Atmos. Chem. Phys.* **2014**, *14*, 10383–10410, DOI:10.5194/acp-14-10383-2014.

37. Wooster, M.J.; Roberts, G.; Perry, G.L.W.; Kaufman, Y.J. Retrieval of biomass combustion rates and totals from fire radiative power observations: FRP derivation and calibration relationships between biomass consumption and fire radiative energy release. *J. Geophys. Res.* **2005**, *110*, D24311, DOI:10.1029/2005JD006318.

38. Madronich, S.; McKenzie, R.E.; Bjorn, L.O.; Caldwell, M.M. Changes in biologically active ultraviolet radiation reaching the earth's surface. *J. Photochem. Photobiol. B:Biology* **1998**, *46*, 5–19.

39. Skamarock, W.C.; Klemp, J.B.; Dudhia, J.; Gill, D.O.; Barker, D.M.; Duda, M.G.; Huang, X.-Y.; Wang W.; Powers, J. G. A Description of the Advanced Research WRF Version 3, *NCAR Tech. Notes–475CSTR*, Boulder, Colorado, USA, 2008; 113 pp.

40. Eskes, H.J.; Boersma, K.F. Averaging kernels for DOAS total column satellite retrievals. *Atmos. Chem. Phys.* **2003**, *3*, 1285–1291, DOI:10.5194/acp-3-1285-2003.

41. Efron, B.; Tibshirani, R.J. *An introduction to the bootstrap*, New York, Chapman & Hall, 1993.

42. Andreae, M.O.; Merlet, P. Emission of trace gases and aerosols from biomass burning. *Glob. Biogeochem. Cy.* **2001**, *15*, 955–966, DOI:10.1029/2000GB001382.

43. Huijnen, V.; Flemming, J.; Kaiser, J.W.; Inness, A.; Leitão, J.; Heil, A.; Eskes, H.J.; Schultz, M.G.; Benedetti, A.; Hadji-Lazaro, J.; Dufour, G.; Eremenko, M. Hindcast experiments of tropospheric composition during the summer 2010 fires over western Russia. *Atmos. Chem. Phys.* **2012**, *12*, 4341-4364, DOI:10.5194/acp-12-4341-2012.